# Enhanced Magneto-Dielectric Properties of 0.6La$_{0.1}$Bi$_{0.9}$FeO$_3$-0.4BaTiO$_3$/NiFe$_2$O$_4$ Composites Sintered with Powders Prepared with a One-Step Sol-Gel *In-Situ* Method

## L. He[*1], J. H. Wang[1], Z. T. Zhong[1], C. Zhang[1]

[1]School of Automation and Information Engineering, Xi'an University of Technology, Xi'an 710048, China

received November 30, 2017; received in revised form January 14, 2018; accepted February 8, 2018

## Abstract

0.6La$_{0.1}$Bi$_{0.9}$FeO$_3$-0.4BaTiO$_3$/NiFe$_2$O$_4$ (0.6LBFO-0.4BT/NFO) composite powders were firstly prepared using a simple one-step sol-gel *in-situ* method. The phase evolution with the calcination temperature was studied. The dense-sintered 0.6LBFO-0.4BT/NFO ceramics were synthesized, and the phase composition as well as the surface morphology were characterized. The dielectric and magnetic properties were measured. The results indicated that with increasing concentration of NFO, the ceramic composite shows an increased dielectric constant ($\epsilon'$) while the dielectric loss tangent (tan $\delta_\epsilon$) value decreases at low frequencies range (in 5 kHz). The magnetic measurement indicates that all the composites show single-phase-like magnetic hysteresis loops and the introduction of NFO can significantly enhance the saturation magnetization (M$_s$) of 0.6LBFO-0.4BT.

*Keywords: Ceramic composites, sol-gel in-situ method, magnetic-dielectric properties*

## I. Introduction

Multiferroic materials with simultaneous electrical and magnetic orderings have attracted significant attention over the past decade because of their fascinating physical properties and potential applications in the emerging field of electromagnetic wave attenuation, data storage media, resistive switching, gas sensors and multi-state memories [1-5]. As an extensively studied single-phase multiferroic material, perovskite BiFeO$_3$ (BFO) exhibits both G-type anti-ferromagnetic and ferroelectric orders in rhombohedrally distorted perovskite structure with the space group of R3c at room temperature [6-8]. The ferroelectricity of BiFeO$_3$ originated from the distortion of the 6S$^2$ lone pair of Bi$^{3+}$ ions, which being largely displaced with the FeO$_6$ octahedra, generates spontaneous polarization along the [111] axis of the rhombohedral unit cell [9-10]. On the other hand, the magnetic property is associated with the residual moment of Fe-site spin structure [11]. However, the difficult preparation, low electrical resistivity and relatively weak magnetism of BFO seriously hinder its practical application in many advanced devices [12-13].

Aiming to overcome the above difficulties, many efforts have been made to enhance the multiferroic properties of BFO. Substituting the A-site Bi$^{3+}$ ions with rare-earth ions (e.g. La$^{3+}$, Pr$^{3+}$ Nd$^{3+}$, Sm$^{3+}$, Dy$^{3+}$) or divalent ions (e.g. Ca$^{2+}$,Ba$^{2+}$) and B-site for Fe$^{3+}$ ions with transition metal ions (e.g. Ni$^{2+}$, Nb$^{5+}$, Sc$^{3+}$) to improve the properties of BFO is viewed as a general method [14-24]. Nevertheless, neither the magnetic nor the ferroelectric properties have improved significantly. Interestingly, recent reports reveal that processing BFO with other perovskite-structured materials (e.g. BaTiO$_3$, PbTiO$_3$) would prevent the formation of secondary phases and enhance the electrical resistivity significantly [25-26]. Moreover, compositing with a strong magnetic phase is a useful method to improve the magnetic properties of BiFeO$_3$ material. NiFe$_2$O$_4$ (NFO) is a well-known cubic ferromagnetic material with soft magnetic character and low magnetic coercivity, which has been studied in detail on account of its high electromagnetic performance, high saturation magnetization, excellent chemical stability and corrosion resistance [27-28]. Whereas, the enhanced multiferroic properties of the composites are difficult to obtain owing to the fact that the multiferroic properties depend on the structures, morphologies, particle size and distribution of the different phases [29-30]. Hence, composite powders with high purity, uniform grain size and uniform distribution of the different phases were essential to the excellent multiferroic properties for the subsequent composites. Obviously, sol-gel *in-situ* methods are commonly used to prepare nanosized composite powders with high purity, uniform grain size and uniform distribution rather than the solid-state reaction process.

In this work, the 0.6LBFO-0.4BT/NFO composite powders were prepared using a simple one-step sol-gel *in-situ* method. The phase evolution with the calcination temperature was studied. Dense-sintered 0.6LBFO-0.4BT/NFO ceramics with different concentrations of NFO were synthesized. The phase composition, sintering behavior, dielectric and magnetic properties were investigated.

* Corresponding author: heli@xaut.edu.cn

## II. Experimental Procedure

The chemical reagents used in this work were $Ba(NO_3)_2$, $Fe(NO_3)_3 \cdot 9H_2O$, $Bi(NO_3)_3 \cdot 5H_2O$, $La(NO_3)_3 \cdot 6H_2O$, $Ni(NO_3)_2 \cdot 6H_2O$, tetrabutyl titanate ($C_{16}H_{36}O_4Ti$), citric acid monohydrate ($C_6H_8O_7 \cdot H_2O$), unsymmetrical dimethylhydrazine ($C_2H_8N_2$), acetic acid ($CH_3COOH$) and ethyl alcohol ($C_2H_5OH$). All the chemicals were of analytical grade purity and were used without further purification.

(1-x)(0.6LBFO-0.4BT)/xNFO composite powders (with x = 0.1, 0.2, 0.3, 0.4) were prepared in a one-step sol-gel *in-situ* process. The preparation process includes the following steps.Stoichiometric amounts of $La(NO_3)_3 \cdot 6H_2O$, $Bi(NO_3)_3 \cdot 5H_2O$, $Fe(NO_3)_3 \cdot 9H_2O$, $Ni(NO_3)_2 \cdot 6H_2O$, $C_6H_8O_7 \cdot H_2O$ were weighed and added into distilled water, which was stirred at room temperature until a brown transparent solution was obtained; a stoichiometric amount of $Ba(NO_3)_2$ was weighed and added into dilute acetic acid to obtain $Ba(NO_3)_2$ solution; a stoichiometric amount of $C_{16}H_{36}O_4Ti$ was weighed and added into ethanol and acetic acid to obtain $C_{16}H_{36}O_4Ti$ solution. Then, the $Ba(NO_3)_2$ solution was added into the $C_{16}H_{36}O_4Ti$ solution slowly until a colorless transparent solution was obtained. Finally, the colorless transparent solution was slowly added into the above-mentioned brown transparent solution, and a certain amount of $C_2H_8N_2$ was added to the solution to inhibit the hydrolyzation of $Ti^{4+}$ and $Bi^{3+}$ ions simultaneously. 5 mol% excess $Bi(NO_3)_3 \cdot 5H_2O$ was added to compensate for Bi loss during the subsequent calcining process. After being magnetically stirred for 2 h, the solution was dried at 200 °C for 2 h to form a black-colored precursor powder. The precursor powders were calcined at 1000 °C for 2 h in air atmosphere to obtain the 0.6LBFO-0.4BT/NFO composite powders. Then, after 5 wt% PVA aqueous solution had been added to the obtained 0.6LBFO-0.4BT/NFO composite powders, these were pressed into disks. Final sintering was performed at 1100 °C for 2 h.

The phase composition of the 0.6LBFO-0.4BT/NFO ceramics was detected with an X-ray diffractometer (XRD) with Cu Kα radiation (Rigaku D/MAX-2400, Japan). The morphology of the samples was analyzed using a scanning electron microscope (SEM) (Hitachi S-4800, Japan) equipped with energy-dispersive X-ray spectroscopy (EDS). The dielectric properties of the samples were measured with an impedance analyzer (E4980A, Agilent, Palo Alto, CA). The magnetic hysteresis loops of the samples were measured with a vibrating sample magnetometer 113 (VSM) (Lake Shore 7410, USA).

## III. Results and Discussion

Fig. 1(a) shows the XRD patterns of the 0.8(0.6LBFO-0.4BT)/0.2NFO powders calcined at different temperatures. It can be seen the calcining temperature has a considerable influence on the phase composition of the composite powders. The raw materials reacted at 750 °C, with the main phases of LBFO-BT and NFO being formed, while the impurity phases of $Bi_2O_3$ and $Fe_2O_3$ existed in the product powders. With the increase in the calcining temperature, the oxides reacted sufficiently with each other and the XRD peaks of main crystal phases are obviously enhanced. The powder product calcined at 900 °C shows pure composite XRD patterns of LBFO-BT and NFO, indicating the principal reaction has been completed. Fig. 1(b) shows the XRD patterns of the 0.6LBFO-0.4BT ceramic, NFO ceramic and 0.6LBFO-0.4BT/NFO ceramics with different concentrations of NFO sintered at 1100 °C for 2 h. All the peaks of 0.6LBFO-0.4BT ceramic and NFO ceramic have been identified from their individual XRD patterns available in the JCPDS data card 73 – 0548 and 54 – 0964 respectively. And the 0.6LBFO-0.4BT phase shows a pure perovskite structure while the NFO phase shows a pure spinel structure. It can also be found that the diffraction peaks of 0.6LBFO-0.4BT/NFO ceramics with all concentrations of NFO corresponded well with the 0.6LBFO-0.4BT ceramic and NFO ceramic. The above XRD patterns reveal that the 0.6LBFO-0.4BT phase and NFO phase can co-exist in the 0.6LBFO-0.4BT/NFO ceramics after being calcined at 1100 °C with a high crystallinity and without any impurity phases. As expected, with increasing the concentration of NFO, the diffraction peaks of NFO become strengthened gradually.
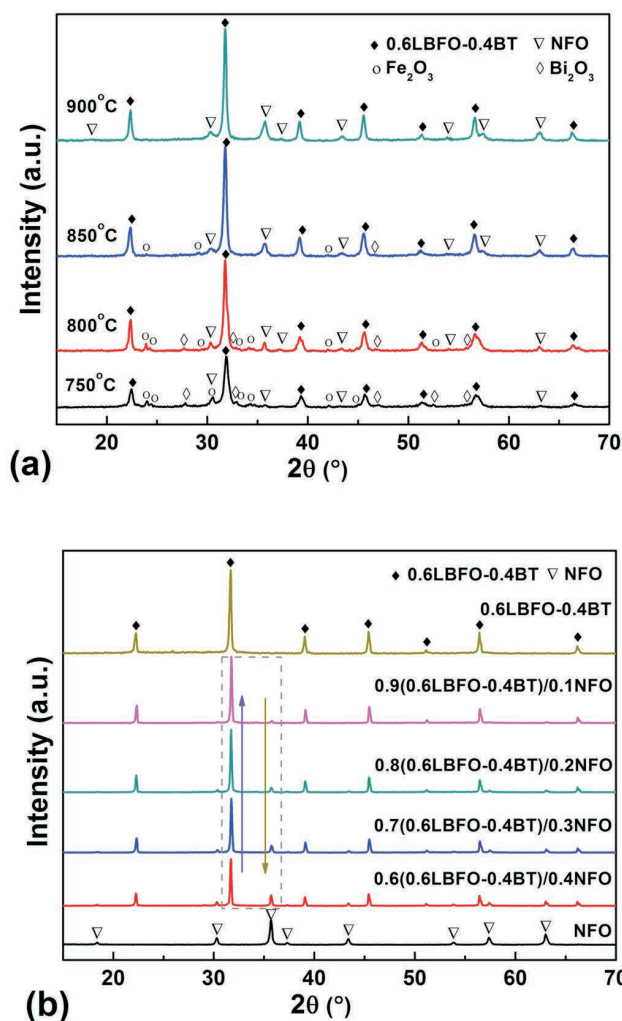


(a)



(b)

**Fig. 1:** XRD patterns of the 0.8(0.6LBFO-0.4BT)/0.2NFO powders calcined at different temperatures (a) and XRD patterns of the 0.6LBFO-0.4BT, NFO and the 0.6LBFO-0.4BT/NFO ceramics with different concentrations of NFO sintered at 1100 °C (b).

Fig. 2 shows the backscattered SEM micrographs of the natural surfaces of the 0.6LBFO-0.4BT/NFO ceramics with different concentrations of NFO sintered at 1100 °C for 2 h. The backscattered SEM can distinguish the 0.6LBFO-0.4BT phase and NFO phase clearly due to the different atomic numbers of the two phases. It can be found that the 0.6LBFO-0.4BT/NFO ceramics consist of white phase and black phase, and it can be inferred that the white phase is 0.6LBFO-0.4BT while the black phase is NFO according to the large atomic numbers of Bi, La, Ba and Ti elements in 0.6LBFO-0.4BT phase and small atomic numbers of Ni, Fe elements in NFO phase. It can also be observed that all the 0.6LBFO-0.4BT/NFO ceramics demonstrated clear phase composition and uniform distribution of the two phases and the number of NFO granular grains increased with increasing concentration of NFO.

To further confirm the composition and distribution of the two phases in the 0.6LBFO-0.4BT/NFO ceramics, Fig. 3 shows the backscattered SEM micrograph, energy spectrum image and the element distribution images of the representative 0.8(0.6LBFO-0.4BT)/0.2NFO ceramic. Similar to Fig. 2, it can be found that the 0.8(0.6LBFO-0.4BT)/0.2NFO ceramic consists of white phase and black phase from the backscattered SEM micrograph. For the energy spectrum diagram, it can be observed that the 0.8(0.6LBFO-0.4BT)/0.2NFO ceramic contains O, Bi, Ba, Ti, La, Fe and Co, seven elements without any other impurity element. In addition, the atomic ratio of Ni/Fe approximately is 0.17, which is very close to the stoichiometric ratio value of 0.22. And the atomic ratio of Bi/Fe approximately is 0.33, which also basically agrees with the stoichiometric ratio value of 0.49. The brightness of the element distribution diagram represents the content of the element on the corresponding position. It can be observed

that the position of the white phase in the backscattered SEM micrograph exhibits relatively high brightness in the Bi, Ba, Ti and La element distribution diagrams, indicating a relatively high content of Bi, Ba, Ti and La elements on the corresponding position, and further confirming the white phase is 0.6LBFO-0.4BT. Moreover, it can be confirmed that the black phase is NFO for the same reason. It can be clearly seen that all the related elements are distributed uniformly in the element distribution diagram, confirming that the two phases are well distributed in the composites. In conjunction with the XRD analysis and the backscattered SEM micrographs, it can be concluded that the 0.6LBFO-0.4BT/NFO ceramics only consist of 0.6LBFO-0.4BT and NFO and the two phases exhibit uniform distribution in the composites.

Fig. 4 shows the frequency dependence of the dielectric properties of the 0.6LBFO-0.4BT ceramic, NFO ceramic and 0.6LBFO-0.4BT/NFO ceramic composites sintered at 1100 °C in the frequency range from 100 Hz to 1 MHz. It can be seen that all the 0.6LBFO-0.4BT/NFO ceramics show similar dielectric behavior at room temperature while the value of ε' decreases gradually with increasing frequency. Higher values of ε' at lower frequencies are due to the presence of the different types of polarization[31] (i.e., dipolar, ionic, electronic, and interfacial) in the ceramics. The main polarization of the 0.6LBFO-0.4BT/NFO ceramics is interfacial polarization at the interface of the two constituents in the ceramics[32]. As the test frequency increases, some of the above-mentioned polarizations cannot follow the alternating field and give a lower contribution to the ε' value. It can also be seen that the value of ε' increases with increasing concentration of NFO owing to the fact that the pure NFO possesses a higher ε' value than 0.6LBFO-0.4BT ceramics.
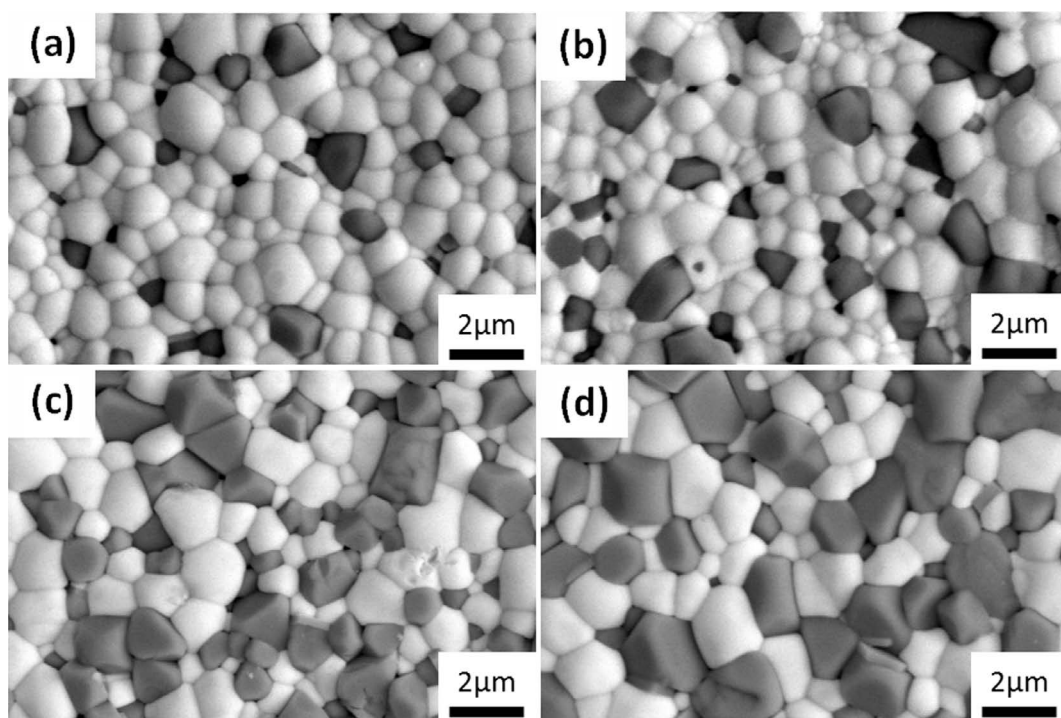


**Fig. 2:** Backscattered SEM of the (1-x)(0.6LBFO-0.4BT)/xNFO ceramics at 1100 °C for 2 h: (a) x = 0.1; (b) x = 0.2; (c) x = 0.3; (d) x = 0.4.
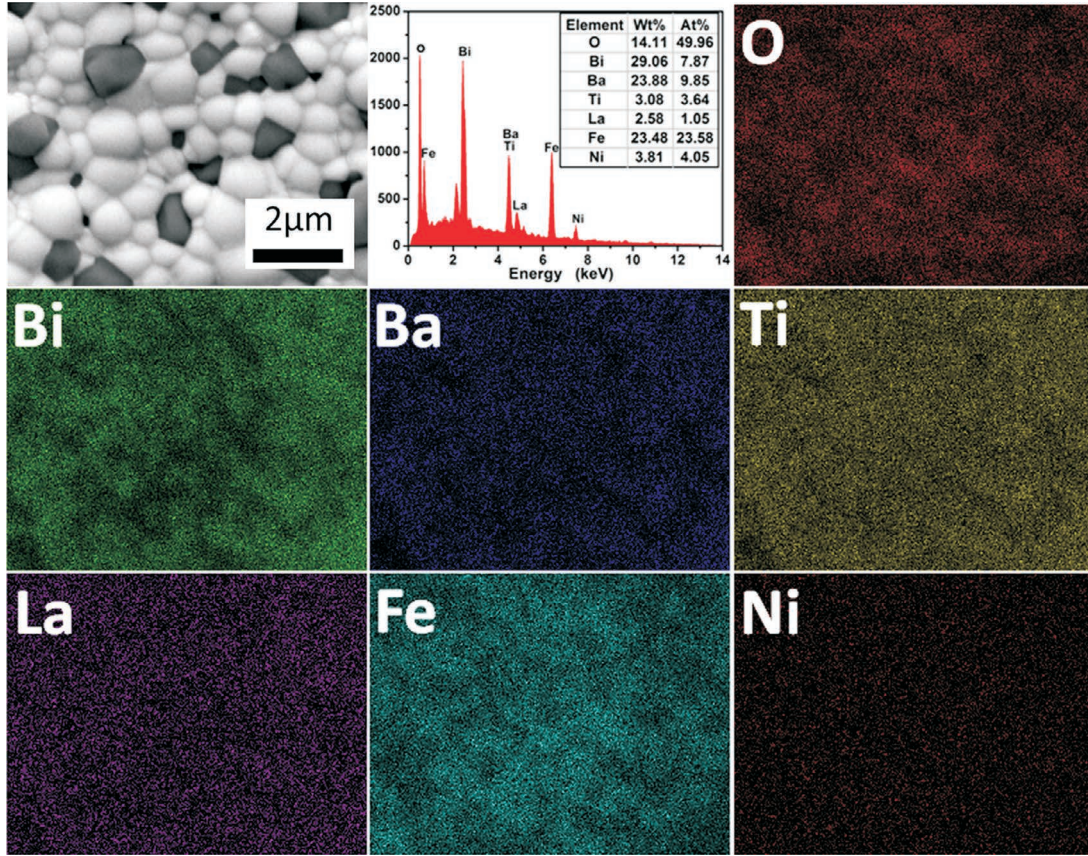
**Fig. 3:** Backscattered SEM micrograph, energy spectrum image and the element distribution images of the representative 0.8(0.6LBFO-0.4BT)/0.2NFO ceramic sintered at 1100 °C for 2 h.
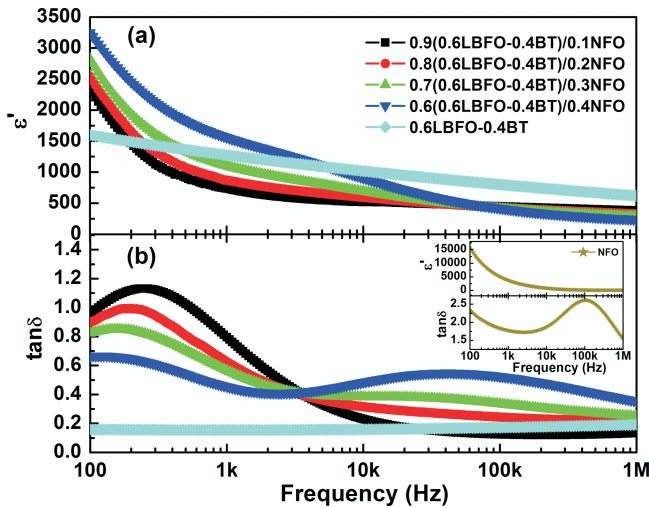


**Fig. 4:** Frequency dependence of the dielectric properties of the 0.6LBFO-0.4BT ceramic, NFO ceramic and the 0.6LBFO-0.4BT/NFO ceramics with different concentrations of NFO sintered at 1100 °C for 2 h.

The value of tan δ decreases with increasing NFO concentration below 5 kHz. When an alternating electric field was applied, there are polarization loss and leakage losses. The dielectric loss can be described by the following Debye formula:

$$D = D_P + D_G = \frac{(\varepsilon_s - \varepsilon_\infty \omega \tau)}{\varepsilon_s + \varepsilon_\infty \omega^2 \tau^2} + \frac{\gamma}{\omega \varepsilon_0} \frac{1}{\varepsilon_\infty + \frac{\varepsilon_s - \varepsilon_\infty}{1 + \omega^2 \tau^2}} \quad (1)$$

where D is the total dielectric loss, $D_P$ is the polarization loss and $D_G$ is the leakage loss, $\varepsilon_s$ and $\varepsilon_\infty$ denote the relative

permittivity of static electrical field and optical frequency, respectively. $\tau$ and $\gamma$ refer to the relaxation time and the conductivity. It can be found that the polarization loss $D_p$ goes to 0 with the frequency ($\omega \to 0$), and in this case, the frequency is low, the tanδ which is almost attributed to the leakage loss and can be approximately described as below:

$$D \cong \frac{\gamma}{\omega \varepsilon_0 \varepsilon_s} \quad (2)$$

Thus, tanδ is inversely proportional to the test frequency in the low-frequency range, which explains why the value of tanδ decreases with the frequency increases at lower frequency. It also explains why the tanδ of 0.6LBFO-0.4BT/NFO ceramics is much higher than that of the pure 0.6LBFO-0.4BT ceramic owing to the decrease of resistivity with the introduction of NFO.

Fig. 5 shows the temperature dependence of the dielectric properties of 0.6LBFO-0.4BT/NFO ceramics with different concentrations of NFO sintered at 1100 °C. For the pure 0.6LBFO-0.4BT ceramic, ε' increases continuously along with the temperature. For NFO ceramic, the dielectric curves demonstrate relaxation behaviors. With the increase of frequency, the value of the ε' deceases while the maximum of ε' shifts to higher temperature. This phenomenon can be explained as follows. The occupations of the $Ni^{2+}$ ions on the octahedral sites and the $Fe^{3+}$ ions on the tetrahedral sites results in the hopping of the charge carriers and the semiconducting nature of the NFO:

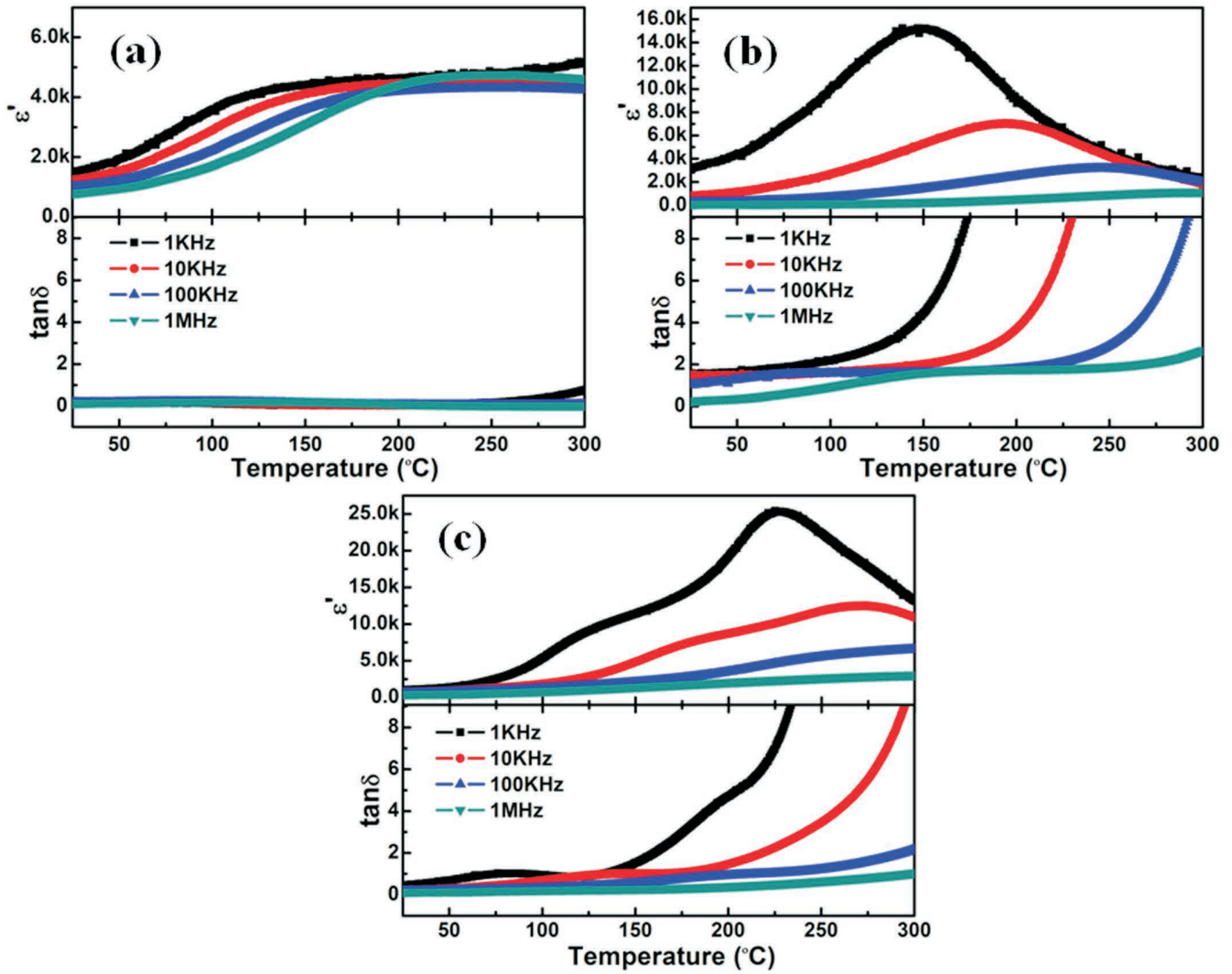$$Ni^{2+} + Fe^{3+} \leftrightarrow Ni^{3+} + Fe^{2+} \quad (3)$$

**Fig. 5:** Temperature dependence of the dielectric properties of the (a) 0.6LBFO-0.4BT ceramic, (b) NFO ceramic and (c) 0.8(0.6LBFO-0.4BT)/0.2NFO ceramic sintered at 1100 °C for 2 h.

This hopping not only contributes to direct current (dc) conductivity, but the dipolar effect [33]. Additionally, with increasing the concentrations of the NFO, the ε' of the composites increases, which results from the lower resistivity of the NFO. Moreover, the relaxation behaviors become apparent.

The room temperature magnetic hysteresis (M-H) loops of the 0.6LBFO-0.4BT, NFO and the 0.6LBFO-0.4BT/NFO ceramics are shown in Fig. 6. It can be seen that all the 0.6LBFO-0.4BT/NFO ceramics show single-phase-like magnetic hysteresis loops, indicating that the 0.6LBFO-0.4BT phase and the NFO phase are well exchange-coupled. Obviously enhanced magnetic properties of the ceramics can be obtained and the $M_s$ increases with increasing concentration of NFO. Table 1 summarizes the saturation magnetization ($M_s$) of the as-prepared 0.6LBFO-0.4BT/NFO ceramics and those of the doped BFO-BT ceramics reported in the literature. It can be clearly seen that all the $M_s$ are much higher than those of the doped BFO-BT ceramics, suggesting that compositing NFO into BFO-BT is a good solution to enhance the magnetic properties of BFO-BT. The details of the hysteresis loops are given in Table 2. The residual magnetism and coerciv-

ity of the ceramics sample are very low, and are close to those parameters of the pure NFO ferrite, indicating that 0.6LBFO-0.4BT/NFO composite is a well-formed soft magnetic material.
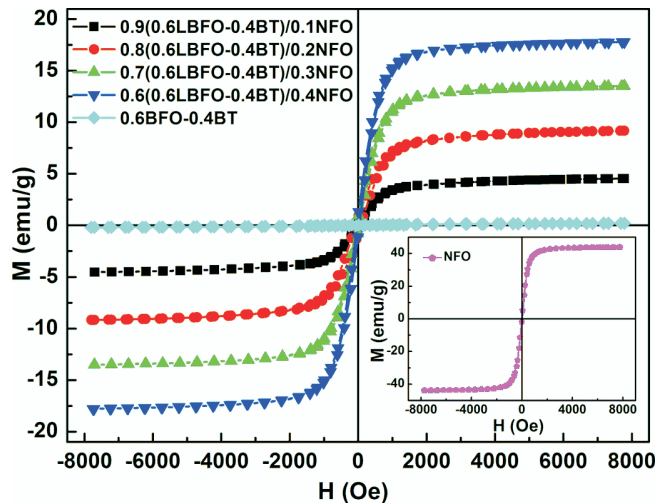


**Fig. 6:** Magnetic hysteresis (M-H) loops of the 0.6LBFO-0.4BT ceramic, NFO ceramic and the 0.6LBFO-0.4BT/NFO ceramics with different concentrations of NFO sintered at 1100 °C for 2 h.

**Table 1:** Saturation magnetization ($M_s$) of doped BFO-BT ceramics and the as-prepared 0.6LBFO-0.4BT/NFO ceramics with different concentrations of NFO.

| Sample | $M_s$(emu/g) | Ref. |
|---|---|---|
| $0.7BiFe_{0.7}Sc_{0.3}O_3$-$0.3BaTiO_3$ | 0.10 | [34] |
| $Bi_{0.75}Ba_{0.25}(Fe,Ti)_{0.95}Mn_{0.05}O_3$ | 0.14 | [35] |
| $Bi_{0.6}Gd_{0.1}Ba_{0.3}Fe_{0.7}Ti_{0.3}O_3$ | 0.34 | [36] |
| $0.85Bi_{0.95}Dy_{0.05}FeO_3$-$0.15BaTiO_3$ | 0.38 | [37] |
| 0.6LBFO-0.4BT | 0.10 | This work |
| 0.9(0.6LBFO-0.4BT)/0.1NFO | 4.16 | This work |
| 0.8(0.6LBFO-0.4BT)/0.2NFO | 8.65 | This work |
| 0.7(0.6LBFO-0.4BT)/0.3NFO | 13.08 | This work |
| 0.6(0.6LBFO-0.4BT)/0.4NFO | 17.35 | This work |

**Table 2:** Magnetic property parameters of the 0.6LBFO-0.4BT/NFO composites with different concentrations of NFO sintered at 1100 °C for 2 h.

| Sample | $M_s$(emu/g) | $M_r$(emu/g) | $H_c$(Oe) |
|---|---|---|---|
| 0.6LBFO-0.4BT | 0.24 | 0.2 | 43 |
| 0.9(0.6LBFO-0.4BT)/0.1NFO | 4.1 | 0.4 | 64 |
| 0.8(0.6LBFO-0.4BT)/0.2NFO | 8.5 | 0.7 | 70 |
| 0.7(0.6LBFO-0.4BT)/0.3NFO | 12.8 | 1.2 | 79 |
| 0.6(0.6LBFO-0.4BT)/0.4NFO | 17.0 | 1.4 | 86 |
| NFO | 43.6 | 2.3 | 93 |

## IV. Conclusions

In conclusion, 0.6LBFO-0.4BT/NFO ceramics were successfully synthesized with a one-step sol-gel *in-situ* method. The XRD, backscattered SEM and EDS analyses reveal that 0.6LBFO-0.4BT and NFO phase can coexist and exhibit clear phase composition of the two phases, uniform distribution and can be dense-sintered. The introduction of NFO has an obvious impact on the dielectric and magnetic performance. The dielectric measurement indicates that the dielectric constant increases while dielectric loss tangent value decreases with increasing concentration of NFO at low frequencies. The magnetic measurement indicates that all the 0.6LBFO-0.4BT/NFO ceramics show single-phase-like magnetic hysteresis loops, and the saturation magnetization ($M_s$) increase with increasing concentration of NFO.

## References

1    Schmid, H.: Multi-ferroic magnetoelectrics, *Ferroelectrics*, **162**, [1], 317–338, (1994).

2    Fiebig, M., Lottermoser, T., Frohlich, D., Goltsev, A.V., Pisarev, R.V.: Observation of coupled magnetic and electric domains, *Nature*, **419**, [6909], 818–20, (2002).

3    Spaldin, N.A., Fiebig, M.: Materials science. the renaissance of magnetoelectric multiferroics, *Science*, **309**, [5733], 391–2, (2005).

4    Eerenstein, W., Mathur, N.D., Scott, J.F.: Multiferroic and magnetoelectric materials, *Nature*, **442** [7104], 759–65, (2006).

5    Kaletsch, A., Bezold, A., Pfaff, E.M., Broeckmann, C.: Effects of copper oxide content in AgCuO braze alloy on microstructure and mechanical properties of reactive-air-brazed $Ba_{0.5}Sr_{0.5}Co_{0.8}Fe_{0.2}O_{3-delta}$ (BSCF), *J. Ceram. Sci. Tech.*, **3**, [2], 95–103, (2012).

6    Neaton, J.B., Ederer, C., Waghmare, U.V., Spaldin, N.A., Rabe, K.M.: First-principles study of spontaneous polarization in multiferroic$BiFeO_3$, *Phys. Rev. B*, **71**, [1], (2005).

7    Wu, J., Xu, J., Li, N., Jiang, Y., Xie, Z.: The phase diagram and magnetic properties of co and ti co-doped (1-x)$BiFeO_3$-$_x$$LaFeO_3$ solid solutions, *J. Alloy. Compd.*, **650**, 878–883, (2015).

8    Simoes, A.Z., Gonzalez, A.H.M., Cavalcante, L.S., Riccardi, C.S., Longo, E., Varela, J.A.: Ferroelectric characteristics of $BiFeO_3$ thin films prepared via a simple chemical solution deposition, *J. Appl. Phys.*, **101**, [7], (2007).

9    Zhao, T., Scholl, A., Zavaliche, F., Lee, K., Barry, M., Doran, A., Cruz, M.P., Chu, Y.H., Ederer, C., Spaldin, N.A., Das, R.R., Kim, D.M., Baek, S.H., Eom, C.B., Ramesh, R.: Electrical control of antiferromagnetic domains in multiferroic $BiFeO_3$ films at room temperature, *Nat. Mater.*, **5**, [10], 823–829, (2006).

10  Yao, Q.R., Cai, J., Zhou, H.Y., Rao, G.H., Wang, Z.M., Deng, J.Q.: Influence of La-doping on structure and magnetic behaviors in BiFeO$_3$, *J. Alloy. Compd.*, **633**, 170–173, (2015).

11  Chybczynska, K., Markiewicz, E., Blaszyk, M., Hilczer, B., Andrzejewski, B.: Dielectric response and electric conductivity of ceramics obtained from BiFeO$_3$ synthesized by microwave hydrothermal method, *J. Alloy. Compd.*, **671**, 493–501, (2016).

12  Selbach, S.M., Einarsrud, M.-A., Grande, T.: On the thermodynamic stability of BiFeO$_3$, *Chem. Mater.*, **21**, [1], 169–173, (2009).

13  Liu, J., Li, M., Hu, Z., Pei, L., Wang, J., Liu, X., Zhao, X.: Effects of ion-doping at different sites on multiferroic properties of BiFeO$_3$ thin films, *Appl. Phys. A-Mater.*, **102**, [3], 713–717, (2011).

14  Basiri, M.H., Shokrollahi, H., Isapour, G.: Effects of la content on the magnetic, electric and structural properties of BiFeO$_3$, *J. Magn. Magn. Mater.*, **354**, 184–189, (2014).

15  Sharma, P., Varshney, D., Satapathy, S., Gupta, P.K.: Effect of pr substitution on structural and electrical properties of BiFeO$_3$ ceramics, *Mater. Chem. Phys.*, **143**, [2], 629–636, (2014).

16  Srivastava, A., Singh, H.K., Awana, V.P.S., Srivastava, O.N.: Enhancement in magnetic and dielectric properties of la and pr co substituted BiFeO$_3$, *J. Alloy. Compd.*, **552**, 336–344, (2013).

17  Wang, D., Wang, M., Liu, F., Cui, Y., Zhao, Q., Sun, H., Jin, H., Cao, M.: Sol-gel synthesis of Nd-doped BiFeO$_3$ multiferroic and its characterization, *Ceram. Int.*, **41**, [7], 8768–8772, (2015).

18  Godara, P., Agarwal, A., Ahlawat, N., Sanghi, S.: Crystal structure refinement, dielectric and magnetic properties of sm modified BiFeO$_3$ multiferroic, *J. Mol. Struct.*, **1097**, 207–213, (2015).

19  Koval, V., Skorvanek, I., Reece, M., Mitoseriu, L., Yan, H.: Effect of dysprosium substitution on crystal structure and physical properties of multiferroic BiFeO$_3$ ceramics, *J. Eur. Ceram. Soc.*, **34**, [3], 641–651, (2014).

20  Yang, C., Liu, C.Z., Wang, C.M., Zhang, W.G., Jiang, J.S.: Magnetic and dielectric properties of alkaline earth Ca$^{2+}$ and Ba$^{2+}$ ions co-doped BiFeO$_3$ nanoparticles, *J. Magn. Magn. Mater.*, **324**, [8], 1483–1487, (2012).

21  Wu, M.S., Huang, Z.B., Han, C.X., Yuan, S.L., Lu, C.L., Xia, S.C.: Enhanced multiferroic properties of BiFeO$_3$ ceramics by Ba and high-valence Nb co-doping, *Solid State Commun.*, **152**, [24], 2142–2146, (2012).

22  Chaudhari, Y.A., Singh, A., Mahajan, C.M., Jagtap, P.P., Abuassaj, E.M., Chatterjee, R., Bendre, S.T.: Multiferroic properties in zn and ni co-doped BiFeO$_3$ ceramics by solution combustion method (SCM), *J. Magn. Magn. Mater.*, **347**, 153–160, (2013).

23  Rao, T.D., Kumari, A., Niranjan, M.K., Asthana, S.: Enhancement of magnetic and electrical properties in Sc substituted BiFeO$_3$ multiferroic, *Physica B*, **448**, 267–272, (2014).

24  Najm, A.A.A., Shaari, A.H., Baqiah, H., Bin Saion, E., Pah, L.K., Kien, C.S., Kechik, M.M.A.: Structural, electrical and magnetic properties of BiFe$_{1-x}$Y$_x$O$_3$ (0 <= x <= 0.6) ceramics, *J. Ceram. Sci. Tech.*, **7**, [4], 329–334, (2016).

25  Zhu, L.-F., Zhang, B.-P., Li, S., Zhao, L., Wang, N., Shi, X.-C.: Enhanced piezoelectric properties of Bi(Mg$_{1/2}$Ti$_{1/2}$)O$_3$ modified BiFeO$_3$-BaTiO$_3$ ceramics near the morphotropic phase boundary, *J. Alloy. Compd.*, **664**, 602–608, (2016).

26  Pang, D., He, C., Han, S., Pan, S., Long, X., Tailor, H.: A new multiferroic ternary solid solution system of BiFeO3-Pb(Fe$_{1/2}$Nb$_{1/2}$)O$_3$-PbTiO$_3$, *J. Eur. Ceram. Soc.*, **35**, [7], 2033–2040, (2015).

27  Naseri, M.G., Saion, E.B., Ahangar, H.A., Hashim, M., Shaari, A.H.: Simple preparation and characterization of nickel ferrite nanocrystals by a thermal treatment method, *Powder Technol.*, **212**, [1], 80–88, (2011).

28  Sarkar, B., Dalal, B., Ashok, V.D., Chakrabarti, K., Mitra, A., De, S.K.: Magnetic properties of mixed spinel BaTiO$_3$-NiFe$_2$O$_4$ composites, *J. Appl. Phys.*, **115**, [12], (2014).

29  Chen, J., Tang, Z., Bai, Y., Zhao, S.: Multiferroic and magnetoelectric properties of BiFeO$_3$/Bi$_4$Ti$_3$O$_{12}$ bilayer composite films, *J. Alloy. Compd.*, **675**, 257–265, (2016).

30  Gao, X., Rodriguez, B.J., Liu, L., Birajdar, B., Pantel, D., Ziese, M., Alexe, M., Hesse, D.: Microstructure and properties of well-ordered multiferroic Pb(Zr,Ti)O$_3$/CoFe$_2$O$_4$ nanocomposites, *Acs Nano*, **4**, [2], 1099–1107, (2010).

31  Dipti, Kumar, P., Juneja, J.K., Singh, S., Raina, K.K., Prakash, C.: Improved dielectric and magnetic properties in modified lithium-ferrites, *Ceram. Int.*, **41**, [2], 3293–3297, (2015).

32  Gul, I.H., Amin, F., Abbasi, A.Z., Anis-ur-Rehmanb, M., Maqsood, A.: Physical and magnetic characterization of co-precipitated nanosize Co-Ni ferrites, *Scripta Mater.*, **56**, [6], 497–500, (2007).

33  Ciomaga, C.E., Airimioaei, M., Nica, V., Hrib, L.M., Caltun, O.F., Iordan, A.R., Galassi, C., Mitoseriu, L., Palamaru, M.N.: Preparation and magnetoelectric properties of NiFe$_2$O$_4$-PZT composites obtained in-situ by gel-combustion method, *J. Eur. Ceram. Soc.*, **32**, [12], 3325–3337, (2012).

34  Shi, C., Liu, X., Hao, Y., Hu, Z.: Structural, magnetic and dielectric properties of sc modified (1-y) BiFeO$_3$-yBaTiO$_3$ ceramics, *Solid State Sciences*, **13**, [10], 1885–1888, (2011)

35  Unruan, S., Srilomsak, S., Priya, S., Jantaratana, P., Rujirawat, S., Yimnirun, R.: Local structure investigation and properties of Mn-doped BiFeO$_3$-BaTiO$_3$ ceramics, *Ceram. Int.*, **41**, [3], 4087–4092, (2015)

36  Rai, R., Bdikin, I., Valente, M.A., Kholkin, A.L.: Ferroelectric and ferromagnetic properties of Gd-doped BiFeO$_3$-BaTiO$_3$ solid solution, *Mater. Chem. Phys.*, **119**, [3], 539–545, (2010).

37  Priya, A.S., Banu, I.B.S., Anwar, S.: Investigation of multiferroic properties of doped BiFeO$_3$-BaTiO$_3$ composite ceramics, *Mater. Lett.*, **142**, 42–44, (2015).